Modeling of percolation of globular-equiaxed grains in Al-Cu alloys

2015 IOP Conf. Ser.: Mater. Sci. Eng. 84 012081

(http://iopscience.iop.org/1757-899X/84/1/012081)

IOP Conf. Series: Materials Science and Engineering **84** (2015) 012081 doi:10.1088/1757-899X/84/1/012081

Modeling of percolation of globular-equiaxed grains in Al-Cu alloys

Christophe Mondoux[1], Hervé Combeau[2], Jean-Luc Desbiolles[1], Michel Rappaz[1]

[1] Department of Materials Science and Engineering, Computational Materials Laboratory (LSMX), Ecole Polytechnique Fédérale de Lausanne, station 12, 1015 Lausanne, CH
[2] Institut Jean Lamour, Departement SI2M, UMR CNRS 7198 Nancy-Université UPVMetz, Ecole des Mines de Nancy, Parc de Saurupt CS 14234, F-54042 Nancy cedex, France

E-mail: christophe.mondoux@epfl.ch

Abstract. A new mesoscopic model able to describe percolation of globular-equiaxed grains, highly relevant for hot tearing formation in castings, has been developed. This model is inspired from the granular model of Sistaninia *et al.* [1–5] that considers polyhedral grains based on a Voronoi tessellation of space. In the new mesoscopic model, the set of tetrahedra that define the grains are further subdivided into smaller tetrahedra called columns and solute diffusion is considered in both the solid and liquid phases. This allows to obtain smoother shapes of the grains and to better describe a progressive coalescence of the grains. In addition, it gives the possibility of having liquid pockets in the last-stage solidification (which is not possible in the case of polyhedral grains) and thus correctly describe the solid fraction at which the grain structure is percolated. The shape of the grains has first been validated with a multiphase-field method. The relevant microstructural features, such as the percolation state of an Al-Cu alloy, were then deduced from the model. This information will then be used to refine the 3D granular models of Sistaninia *et al.* [1–5] which account for stress development and liquid feeding, in order to create more advanced predictive tools for hot tearing formation.

1. Introduction

Hot tearing is a major defect of solidification and welding processes that occurs in metallic alloys while they are in the semi-solid state [6, 7]. The two main phenomena leading to hot tearing are: a lack of liquid feeding at high solid fractions and tensile/shear strains in the mushy zone that tend to pull apart the solid network. The strains, transmitted through the partially coherent solid in the mushy zone, are induced by contraction of the solid in a thermal gradient, and mechanical constraints imposed by the geometry of components. At low solid fraction ($g_s < 0.9$), the permeability of the mushy zone is large enough so that liquid feeding can heal possible grain boundary openings, forming a so-called *healed hot tear*. At high solid fraction ($g_s > 0.95$) the grains form a continuous solid network possessing sufficient mechanical resistance and the mushy material behaves as a ductile solid. However, there is a critical zone for hot tearing (for solid fractions in the range of $0.9 < g_s < 0.95$) in which grain boundaries openings, due to the deformation localized at those which have still a liquid film, cannot be fed by liquid flow because of the low permeability of the mushy zone [8]. Therefore, it is important to know when the solid grains coalesce and percolate to form a fully coherent solid, i.e., when

the material can transmit stresses and strains but also withstand thermal contraction without rupture [8,9]. Coalescence is defined as the disappearance of a liquid film in between two distinct grains, forming a solid grain boundary, while percolation is defined as the gradual transition of isolated grains or clusters surrounded by a continuous liquid film to a continuous solid network across a domain, even if some liquid regions remain [9, 10].
Coalescence is strongly influenced by the interfacial energies. In the case of a thin liquid film that separates two coalescing grains, as the thickness of the liquid film approaches the solid/liquid interface thickness, $\delta_{s\ell}$, the excess free energy deviates from the initial value of $2\gamma_{s\ell}$, where $\gamma_{s\ell}$ is the energy of the solid/liquid interface. When the liquid has completely disappeared, the excess free energy is equal to the grain boundary energy γ_{gb} [9]. In the case $\gamma_{gb} > 2\gamma_{s\ell}$, the substitution of two solid/liquid interfaces by a grain boundary is associated with an increase of the excess interface energy: a bridging undercooling, ΔT_b, is thus necessary to coalesce the two interfaces (repulsive case). On the other hand, in the case $\gamma_{gb} < 2\gamma_{s\ell}$, no undercooling is needed to coalesce the two interfaces (attractive case). The bridging undercooling needed for the coalescence of a repulsive grain is given by [9]:

$$\Delta T_b = \frac{\gamma_{gb} - 2\gamma_{s\ell}}{\Delta S_f} \frac{1}{\delta_{s\ell}} \tag{1}$$

where ΔS_f is the volumetric entropy of fusion. For a binary alloy, the situation is more complex, because the solute element can alter the grain boundary energy but also mainly because coalescence is influenced by the solute concentration in the liquid film. The rejection and diffusion of solute in the liquid parallel to the film as well as back-diffusion perpendicular to the impinging interfaces can thus play an important role [9]. Coalescence will occur when the temperature and the concentration of the liquid film reaches a so-called *coalescence line*, which is parallel to liquidus line in the phase diagram, but shifted down by ΔT_b.

2. Model

We propose a new mesoscopic model inspired from the 3D polyhedral granular model developed in [1–5], in order to obtain smoother grain morphologies compared to those reported in [1–5] and to predict more accurately the percolation state for a large population of grains. As for the granular model, a Voronoi tessellation is generated from randomly distributed nucleation centers. However, instead of considering the pyramids in 3D (sectors in 2D) having a nucleation center as a summit and the Voronoi facets as bases (see Fig. 1(a) and 1(b)), each of them is subdivided into several columns (see Fig. 1(c) and 1(d)). The liquid composition at the interface $c^*_{\ell,i}$, in column i, possessing a mean curvature $\overline{\kappa}_i$ at a given temperature T (supposed uniform over the calculation domain) is given by:

$$c^*_{\ell,i}(T,\kappa) = -\frac{T_m - T - \Gamma_{s\ell}\overline{\kappa}_i}{m_\ell} \tag{2}$$

where T_m is the melting point of pure aluminum, $\Gamma_{s\ell}$ the Gibbs-Thompson coefficient, and m_ℓ the liquidus slope. Altough small for globular grains (a few mK), the curvature contribution is still necessary because it stabilizes the s-ℓ interface, as expected, by inducing a flow of solute from low to high curved regions.
Within each column i, backdiffusion in the solid is calculated radially by using a Landau transformation of the domain $r \in [0, r^*_i(t)]$ (where r is the distance and r^*_i the distance of the interface from the nucleation center of the grain in the column i) into a reference domain $\eta \in [0, 1]$, as introduced by Voller and Sundarraj [11]. The concentration of the solid $c_{s,i}$ becomes:

$$c_{s,i}(r,t) \rightarrow c_{s,i}(\eta,t) \quad \eta = \frac{r}{r^*_i(t)} \tag{3}$$

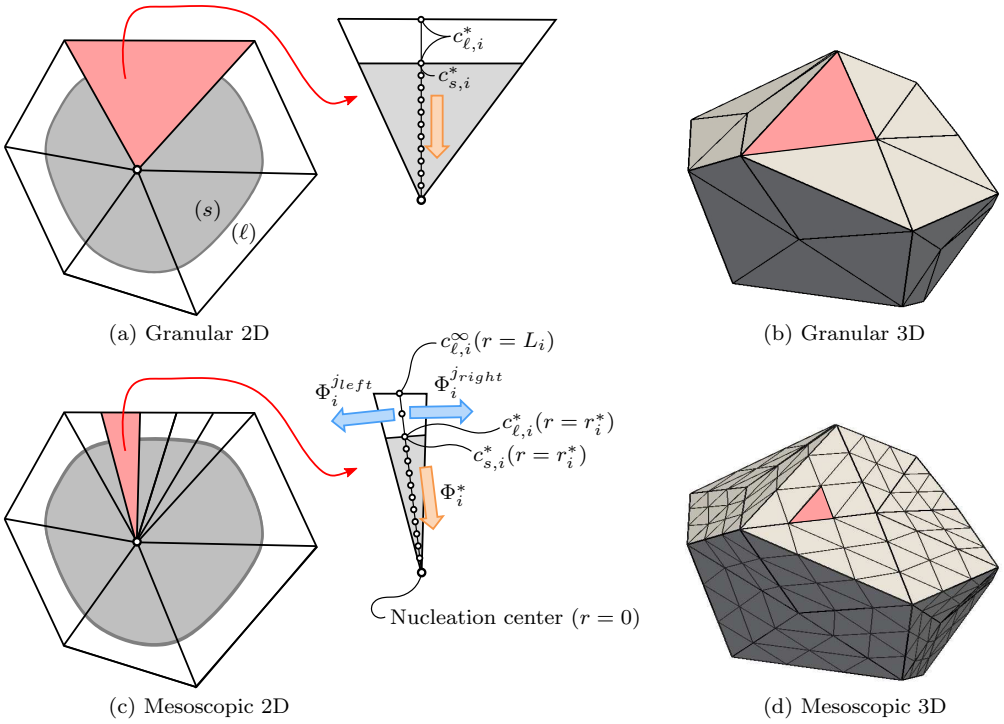

(a) Granular 2D (b) Granular 3D

(c) Mesoscopic 2D (d) Mesoscopic 3D

Figure 1: Schematic representation of the polyhedral granular model of Sistaninia *et al.* [1–5] compared to the present smooth granular model.

The diffusion equation in the solid thus becomes:

$$\left(\frac{\partial c_{s,i}}{\partial t}\right)_\eta = \frac{D_s}{r_i^{*2}}\frac{\partial^2 c_{s,i}}{\partial \eta^2} + \left(\frac{\eta v_i^*}{r_i^*} + \frac{(P-1)D_s}{\eta r_i^{*2}}\right)\frac{\partial c_{s,i}}{\partial \eta} \tag{4}$$

where v_i^* is the velocity of the interface, D_s the diffusion coefficient of the solid phase and P the dimension of the problem (3 for 3D and 2 for 2D). Eq. (4) is solved using an implicit finite difference scheme. By integrating the concentration of the solid, one can thus find the flow of solute pumped by the solid at the interface, Φ_i^*:

$$\Phi_i^* = \frac{d}{dt}\int_0^{r_i^*(t)} c_{s,i} dV = \int_0^{r_i^*(t)} \frac{\partial c_{s,i}}{\partial t} dV + c^*_{s,i}\frac{dr_i^*}{dt} S_i^* \tag{5}$$

where S_i^* is the area of the surface separating the liquid and the solid parts of the column i. In the liquid part of the column, the liquid concentration, $c_{\ell,i}$, is assumed to be a piecewise parabolic-linear function:

$$c_{\ell,i}(r) = \begin{cases} c^\infty_{\ell,i} + \left(c^*_{\ell,i} - c^\infty_{\ell,i}\right)\left(\frac{\lambda_i - (r - r_i^*)}{\lambda_i}\right)^2 & \text{if} \quad r < r_i^* + \lambda_i \\ c^\infty_{\ell,i} & \text{if} \quad r \geqslant r_i^* + \lambda_i \end{cases} \tag{6}$$

where $c^\infty_{l,i} = c_{l,i}(r = L_i)$ is the concentration at the Voronoi facet and λ_i the diffusion layer thickness. Before the diffusion layer reaches the Voronoi facet, $c^\infty_{\ell,i}$ is set to the nominal concentration and λ_i can be found by knowing the average concentration in the liquid part of the column $\langle c_{\ell,i}\rangle$. Once the diffusion layer has reached the Voronoi facet, λ_i is known and

equal to $L - r_i^*$ while $c_{\ell,i}^{\infty}$ is unknown and can be found from $\langle c_{\ell,i} \rangle$. Note that the approximation of the profile in the liquid by a piecewise parabolic-linear function does not correspond to the solution of the diffusion equation in cylindrical or spherical coordinates. However, when the diffusion layer has reached the Voronoi facet, the derivative at $r = L_i$ is zero and it is thus consistent with the fact that there is a symmetric column on the other side of the Voronoi facet imposing a no-flux condition.

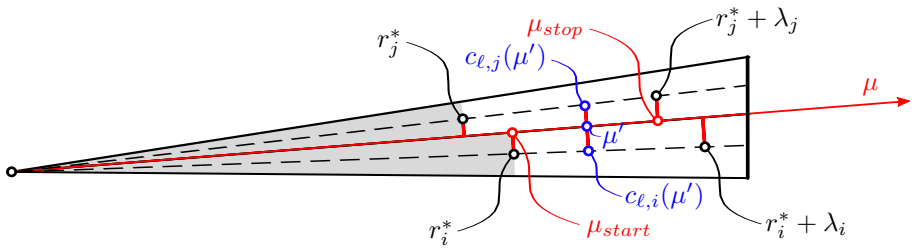

Figure 2: Schematic representation of the calculation of diffusion in the liquid between two adjacent columns.

Then, the flow of solute exchanged between two columns is calculated. Let us define μ as the distance with respect to the nucleation center along the surface separating the two columns (see Fig. 2). The flow of solute is evaluated by calculating the difference in liquid concentration between the columns perpendicularly to the μ-axis. In 2D, the flow of solute leaving the liquid part of column i and going into the adjacent liquid part of column j is given by:

$$\Phi_i^j = -\int_{\mu_{start}}^{\mu_{stop}} D_\ell \frac{c_{\ell,j}(\mu') - c_{\ell,i}(\mu')}{d_{\mu'}} dS_{lat} \tag{7}$$

where D_ℓ is the diffusion coefficient in the liquid, S_{lat} corresponds to the lateral surface through which solute is exchanged (in 2D, $dS_{lat} = d\mu'$) and $d_{\mu'}$ the distance between the positions at which the concentrations are evaluated in the adjacent columns. μ_{start} and μ_{stop} are defined as follows: the two positions corresponding to r_i^* and r_j^* are projected onto the μ axis. The projected position that is the furthest away from the nucleation center is set as μ_{start}. On the other hand, μ_{stop} is defined as the position of the projection of $r_i^* + \lambda_i$ and $r_j^* + \lambda_j$ that is the closest to the nucleation center. In 3D, the method is similar but the surface of the facet separating the two columns as well as the angle with the normal of the facet are taken into account in Eq. (7).

The change of the average concentration in the liquid is thus given by substracting the flow exchanged with the solid part of the column and with the liquid parts of the adjacent columns:

$$\frac{d}{dt}\int_{r_i^*}^{L_i} c_{\ell,i}\, dV = -\left(\Phi_i^* + \sum_{j=\text{neighbour}} \Phi_i^j\right) \tag{8}$$

Please note that the back-diffusion in the solid is purely 1-dimensional in this model, i.e., no direct exchange of solute between the solid parts of the columns and between the solid and liquid parts of different columns. In fact, the solute exchanged is assumed to take place only between the liquid parts of adjacent columns.

The velocity of the interface can then be found by a solute balance at the interface:

$$v_i^* = \frac{1}{(1-k_0)c_\ell^*}\left(D_s\left[\frac{\partial c_s}{\partial r}\right]^* + D_\ell \frac{c_{\ell,i}^* - c_{\ell,i}^{\infty}}{h_i}\right) \tag{9}$$

k_0 is partition coefficient and $\left[\frac{\partial c_s}{\partial r}\right]^*$ is estimated numerically. h_i corresponds to $\lambda_i/2$ until the solute layer has reach the Voronoi facet. When this occurs, the position (and thus the velocity) of the interface can be deduced from an overall solute balance at the level of one column. Once the velocity is known, the whole calculations can be made again starting from Eq. (4) for the next timestep.
Near the end of solidification, once two solid-liquid interfaces get in close contact, when the liquid layer thickness becomes lower than $\delta_{s\ell} = 1$nm, the liquid layer thickness is fixed to $\delta_{s\ell}$ and the concentration of the liquid is supposed to be uniform within the liquid part of each column and is not anymore linked to the phase diagram with Eq. (2). Essentially, the liquid concentration will decrease (by backdiffusion of solute in the solid perpendicular to the interface and diffusion in the liquid from adjacent columns parallel to the interface). Once the coalescence line is reached, the two interfaces have coalesced.

3. Results

3.1. Validation

First, the model has to be validated with a more refined model, such as the multiphase-field method [12]. A multiphase-field formulation, based on the work of Meidani *et al.* [13], has been developed in order to describe the evolution of the shape of the grains and also, unlike the standard phase-field method, to consider grain boundary energies, by assigning a different phase field variable to each grain. The validation has been performed in simple cases where a single grain grows in a square (2D) or cubic (3D) domain (see Fig. 3).

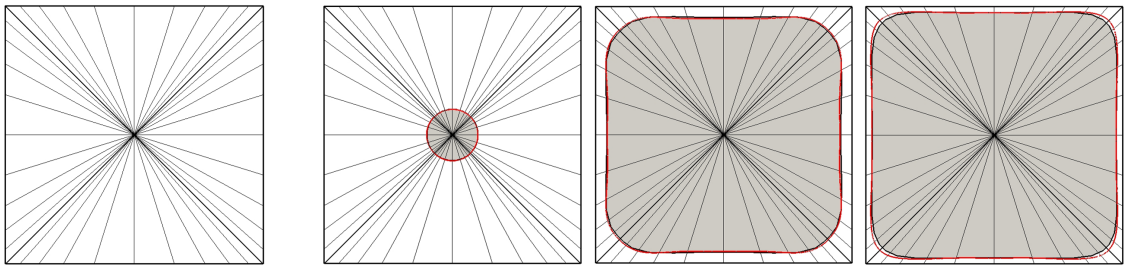

(a) Meshing of the triangles into columns

(b) Evolution of a single 2D grain

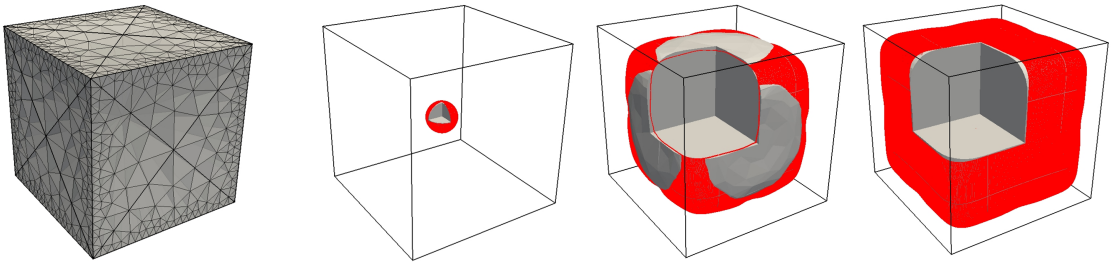

(c) Meshing of the tetrahedra into columns

(d) Evolution of a single 3D grain

Figure 3: (a) and (c) Meshing of the triangles/tetrahedra into smaller columns. (b) and (d) Comparison of grain evolution computed by the mesoscopic model (in gray) and the multiphase-field model (in red).

Note that the meshing in both 2D and 3D is more refined closer to the edges, i.e. the places where a higher curvature is expected near the end of solidification. The mesoscopic model is in a good agreement with the multiphase-field model in both 2D and 3D. In fact, the mesoscopic model

captures correctly the physics of solute diffusion, since the shapes of the grains are really close, as long as there is no strong intability of the solid-liquid interface (i.e., small grain size) [14]. In addition, as the multiphase-field method, the mesoscopic model predicts the fact that, at the center of the flat parts of the grains, the interface is slightly negatively curved towards the center of nucleation of the grain.

3.2. 2D results

It is then interesting to follow the evolution of a large number of grains. In Fig. 4, one can observe the solidification of a set of 1024 randomly nucleated grains (possessing an average size of 100μm) in 2D for an Al-1wt%Cu alloy cooled at -1°C/s. The progressive formation of grain clusters can be tracked following two different criteria. With the contact criterion, two grains belong to the same cluster when the thickness of the liquid film separating them attains $\delta_{s\ell}$ (*contact clusters*). With the coalescence criterion, two grains belong to the same cluster when they are locally coalesced (*coalescence clusters*). The *grain contact* onset time is defined as the time at which the first two grains get into contact.

As shown in figure 5, the number of contact clusters decreases faster than the coalescence clusters, since the coalescence criterion is more restrictive. This can be seen in particular at 534°C, where the solid structure becomes fully percolated for both criteria but there is a single cluster only with the contact criterion. In reality at 548°C, the eutectic would have filled the remaining liquid space (if the second phase can nucleate), but the model allows to find the solidification of eutectic-free alloys. Another way of tracking the progressive percolation of grains is to observe the evolution of the solid liquid interfacial area per unit volume, $S_{s\ell}/V$. This value has been

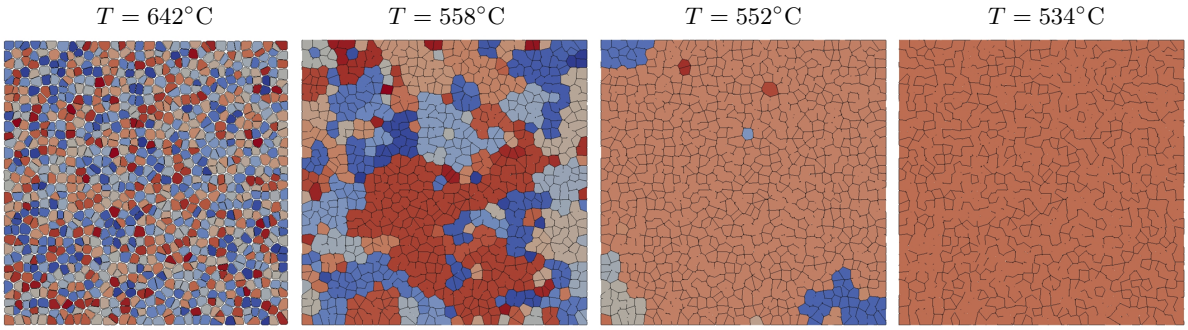

(a) Grain clusters with the contact criterion

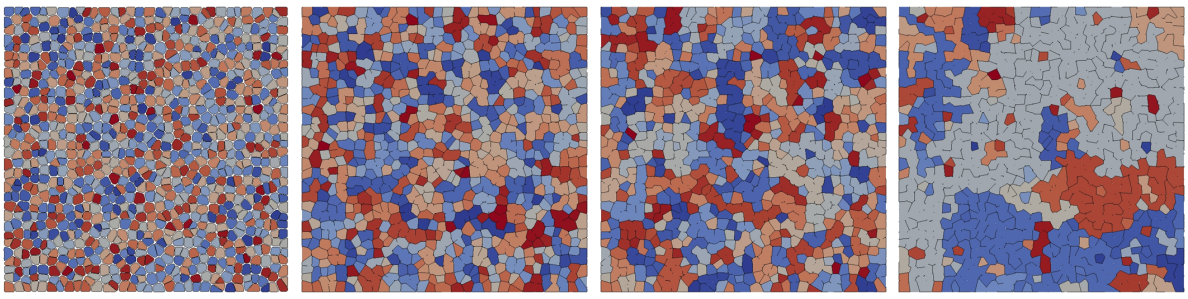

(b) Grain clusters with the coalescence criterion

Figure 4: 2D percolation of an Al-1wt%Cu specimen containing 1024 grains. The average grain size was set to 100μm. Each grain cluster is represented by a different color and the grains clusters are either defined by (a) the contact criterion and (b) the coalescence criterion. The solid/liquid interface is represented by black segments.

normalized by the average grain size, d_{grain}, in order to obtain $\mathcal{S}_{s\ell} = \frac{S_{s\ell} d_{\text{grain}}}{V}$. The evolution of $\mathcal{S}_{s\ell}$ of the model as a function of the solid fraction initially increases because of grain growth, but then decreases abruptly as a solid fraction $g_s = 0.975$ when grain coalescence becomes significant. It is interesting to note that, until significant coalescence takes place, the evolution of $\mathcal{S}_{s\ell}$ closely follows the predictions of a regular arrangement of hexagonal grains.

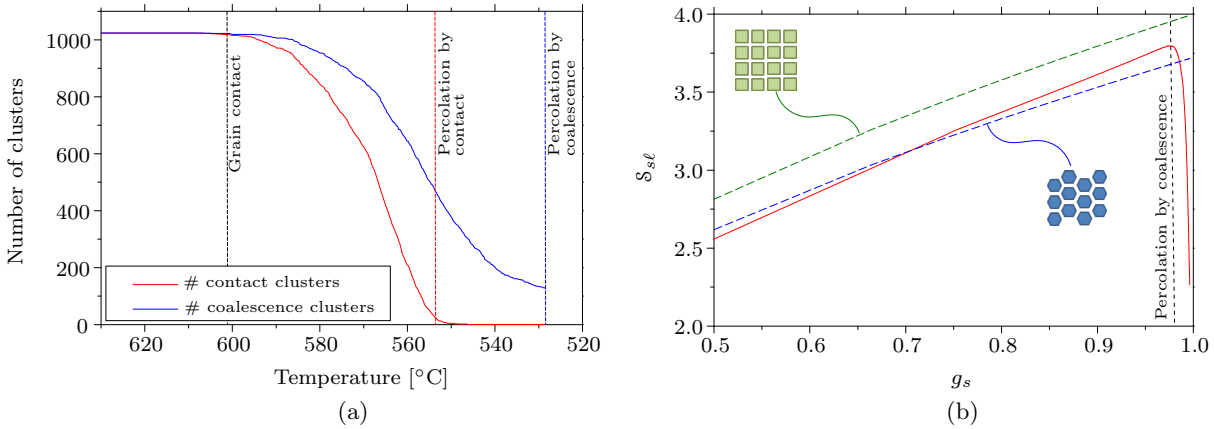

Figure 5: (a) Evolution of the number of clusters as a function of temperature (the grain contact temperature and the temperatures at which the structure is percolated following the two criteria are also indicated). (b) Evolution of $\mathcal{S}_{s\ell} = \frac{S_{s\ell} d_{\text{grain}}}{V}$ as a function of the solid fraction, g_s. The mesoscopic model result is shown in red, while the analytical predictions for a regular arrangement of square and hexagonal grains are in green and blue respectively.

3.3. 3D results

The model was extended in 3D and one preliminary result is shown in Fig. 6, where the progressive percolation of grains can be observed as solidification proceeds. It is interesting to note how the liquid pockets (possessing a negative mean curvature) are formed at the end of

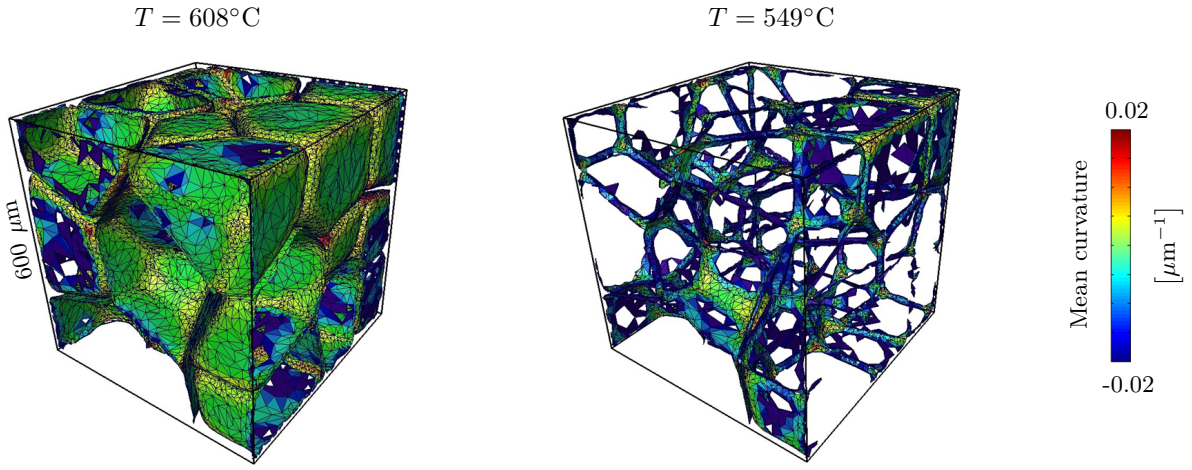

Figure 6: Simulation of the solidification of 3x3x3 grains of an Al-3wt%Cu cooled at -0.05°C/s. The grain size was fixed to 200μm.

solidification. The formation of the liquid pockets in fact is an indication of coalescence, since, when two grains coalesce, part of their solid/liquid interface disappears and only some liquid eventually remains at the corner of the grains.

4. Conclusion

The new mesoscopic model has been successfully validated with a multiphase-field model, in both 2D and 3D for simple domain geometries. This indicates that the assumptions of the mesoscopic model, in particular neglecting direct exchange of solute between the solid parts of the columns and the assumption of a piecewise parabolic-linear profile in the liquid, are reasonable.
In 2D, the mesoscopic model was able to correctly describe the percolation transitions of a large number of grains and currently a benchmark of the percolation transition values for different alloys and cooling conditions is being performed in order to assess the influence of the nominal composition and cooling rates. In 3D, the model predicts the formation of liquid pockets but need to be compared with 3D experimental results.

5. Acknowledgments

The authors gratefully acknowledge the support of the Swiss National Fund (Grant Nos. 200020-132848 and 200020-146879).

References

[1] Phillion A, Vernède S, Rappaz M, Cockcroft S and Lee P D 2009 *Intern. Journ. of Cast Met. Res.* **22** 240-3
[2] Sistaninia M, Phillion A, Drezet J M and Rappaz M 2011 *Met. and Mat. Trans. A* **42** 239-48, 2011
[3] Sistaninia M, Phillion A, Drezet J M and Rappaz M 2012 *Acta Mater.* **60** 3902-11
[4] Sistaninia M, Phillion A, Drezet J M and Rappaz M 2012 *IOP Conf. Ser.: Mat. Sci. and Eng.* **33** 012070
[5] Sistaninia M, Phillion A, Drezet J M and Rappaz M 2012 *Acta Mater.* **60** 6793-803
[6] Campbell J 2003 *Castings (second edition)* Elsevier
[7] Dantzig J A and Rappaz M 2009 *Solidification* EPFL Press
[8] Rappaz M, Drezet J M and Gremaud M 1999 *Met. and Mat. Trans. A* **30** 449-55
[9] Rappaz M, Jacot A and Boettinger W 2003 *Met. and Mat. Trans. A* **34** 467-79
[10] Vernède S and Rappaz M 2006 *Phil. Mag.* **86** 3779-94
[11] Voller V R and Sundarraj S 1993 *Mat. Sci. and Tech.* **9** 474-82
[12] Steinbach I, Pezzolla F, Nestler B, Seeßelberg M, Prieler R, Schmitz G and Rezende J 1996 *Physica D: Nonlin. Phen.* **94** 135-47
[13] Meidani H and Jacot A 2011 *Acta Mater.* **59** 3032-40
[14] Diepers H J and Karma A 2004 *Solidif. Proc. and Microstr.: A Symp. in Honor of Prof. W. Kurz* **369**